SOAC Project − ENSO recharge Oscillator

Peter Farrell, Dong Jian

January 6, 2022

Abstract

The Recharge Oscillator model developed by Jin (1997) represents one way in which El Niño–Southern Oscillation (ENSO) is created and sustained. In this report, we investigate the robustness of this model by starting with its simplest implementation and progressively including additional effects. We begin by analysing a linear, coupled set of equations that relate thermocline anomaly in the west equatorial Pacific to sea surface temperature (SST) anomaly in the east equatorial Pacific. We then introduce non-linearity and stochastic wind forcing. Wind forcing is parameterised by a simple annual oscillation, then given complexity through the inclusion of stochastic forcing. Forcings due to uncorrelated white noise and autocorrelated red noise are investigated. An extended model with nonlinearity and stochastic wind forcing is found to result in an ENSO-like simulation where the duration, intensity, and overall variability approach that seen in observations. Limitations to this approach are also discussed, and an overview is given of future directions for this project.

Introduction

El Niño–Southern Oscillation (ENSO) is an irregular periodic oscillation in sea surface temperature (SST) and equatorial trade winds that occurs in 2-7 year cycles. The interannual fluctuation of the ENSO system comprises alternating warm and cold phases, where temperature and thermocline anomalies shift between the west and middle or east equatorial Pacific. ENSO affects the global weather and climate, and efforts to predict it can be of enormous importance, especially considering effects on ecosystems and the economy.

The oceanic phenomenon was first described in the 19th Century by fishermen in the East Pacific who noticed periods of more extreme weather every few years, and was christened *corriente del niño* (the current of the boy child) by since it usually occurred around Christmas [Carrillo (1892)]. While investigating the Indian Monsoon, an atmospheric oscillation between the Indian and Pacific Oceans that became known as the Southern Oscillation was discovered [Walker (1924)], and later specifically linked to El Niño [Bjerknes (1969)]. The two phenomena are now regarded as a single ocean-atmosphere oscillation, and indices characteristic of these phenomena have a typical correlation of approximately 0.9 [Wright et al. (1988)].

The prevailing winds in the Pacific are the easterlies or trade winds. Therefore, the Sverdrup transport is convergent in the east, leading to upwelling of cold water; and there is divergence in the west, where winds rise, and water is forced away from the equator. This leads to a build-up of heat energy in the west, and a shoaling in thermocline height. So, the west equatorial Pacific is usually warm and has a deeper than average thermocline, while the east equatorial Pacific is cool and has a shallower than average thermocline. In fact, there is a pronounced *cold tongue* of anomalously cool water stretching from the East to the Middle Pacific.

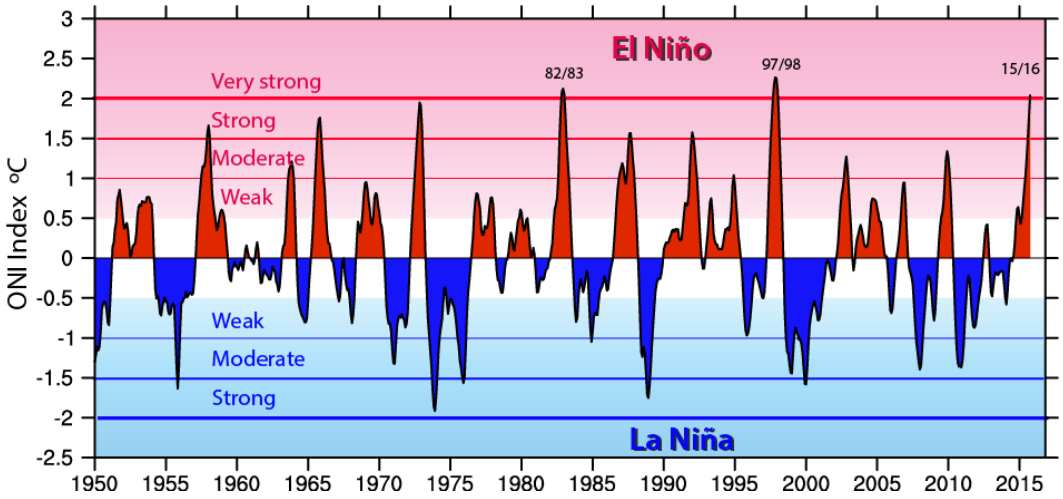

Figure 1: Oceanic Nino Index (1950-2016). El Niño and La Niña phases are given in blue and red respectively. These phases oscillate chaotically in a manner that is difficult to predict. [Trenberth et al. (2020)]

El Niño occurs when the usually cool eastern equatorial Pacific becomes anomalously warm, leading to greater precipitation and storms in the East and droughts in the West. The opposite, La Niña, occurs when the western equatorial Pacific becomes anomalously warm, leading to even greater precipitation in the West and drought in the East. Bjerknes (1969) realised that an intensified Walker Circulation could explain the origins of El Niño. Anomalously cool waters in the East Pacific would lead to more intense easterlies, which in turn would lead to greater heat content in the West Pacific, a deeper thermocline overall, and more convection above the West Pacific. This warm air that is convected to the upper branch of the circulation would return to the East, then sink and promote greater cold water upwelling and reinforce the overall cycle, leading to a positive feedback. What was still not clear, however, was what could act to destroy the positive feedback and tip the system to the other phase.

There are a number of theories as to why and how ENSO changes phase [Timmerman et al. (2018)], but the one we will discuss in this report is the Recharge Oscillator Model. In this model, respective phases build up (recharge) to a certain heat content or thermocline depth, then discharge their energy through ocean adjustment processes, returning to a neutral ocean-atmosphere state before tipping to the other state.

The Recharge Oscillator Model

The Recharge Oscillator Model used in this report is based on the model developed by Jin (1997). This model uses two coupled, non-dimensionalized variables: the sea surface temperature (SST) anomaly in the equatorial eastern Pacific T_E and the thermocline depth anomaly in the equatorial western Pacific h_W. These variables are coupled, the degree to which being determined by a coupling coefficient μ. As with T_E and h_W, μ and other parameters are non-dimensional. Figures may be rendered in non-dimensional terms; however, it was decided to re-dimensionalize the output. One non-dimensional time step is equal to two months.

We start with a linear, coupled model given below in Equations 1 and 2.

$$\frac{dT_E}{dt} = RT_E + \gamma h_W \tag{1}$$

$$\frac{dh_W}{dt} = -rh_W - \alpha b T_E \tag{2}$$

These equations express the coupled time evolution of T_E and h_W respectively. The extent to which they are coupled is determined by b − itself a product of the coupling coefficient μ and a high-end value for coupling b_0 (usually 2.5).

$$b = b_0 \mu \tag{3}$$

R represents Bjerknes Feedback, and may be considered as the growth rate of T_E. It is defined below in Equation 4.

$$R = \gamma b - c \tag{4}$$

r represents the damping rate of h_W, and as such is the growth rate of h_W. The second term in Equations 1 and 2 are controlled respectively by the parameters γ and α. These parameters moderate the coupling between T_E and h_W: γ involves the thermocline feedback and α refers to the slow equatorial recharge-discharge process associated with oceanic heat transport.

The simple model given above (Equations 1 and 2) may be extended by the addition of a nonlinear term $\epsilon(h + bT)^3$ that represents ocean-atmosphere nonlinear processes with ϵ being a nonlinearity parameter (between 0 and 1). The equations become

$$\frac{dT_E}{dt} = RT_E + \gamma h_W - \epsilon(h + bT)^3 \tag{5}$$

$$\frac{dh_W}{dt} = -rh_W - \alpha b T_E \tag{6}$$

Subsequent analysis may be undertaken by factoring in the effect of wind forcing ξ. The equations then become

$$\frac{dT_E}{dt} = RT_E + \gamma h_W - \epsilon(h_W + bT_E)^3 + \gamma\xi \tag{7}$$

$$\frac{dh_W}{dt} = -rh_W - \alpha b T_E - \alpha\xi \tag{8}$$

This wind forcing can be analysed in two ways. Firstly, we investigate the effects of an annual cycle in wind forcing; then, we investigate what happens when stochastic forcing is incorporated into the annual cycle. In the first case, we assume that the wind may be approximated by an sinusoidal annual cycle as in Equation 9, with an annual forcing f_{ann} (a value between 0 and 1). This term principally represents the deviation of wind from the dominant easterly vector.

$$\xi = f_{ann} \cos\left(\frac{2\pi t}{\tau}\right) \tag{9}$$

In the second case, we examine the effects of adding stochastic wind forcing, which represents real weather noise. This effect is included in Equation 10, where we can see that an additional term has been added: W is a random number between -1 and 1 that represents *white noise*, τ_{cor} is a time interval taken here to be one, and f_{ran} is a controlling parameter taken to be 0.1.

$$\xi = f_{ann} \cos\left(\frac{2\pi t}{\tau}\right) + f_{ran} W \frac{\tau_{cor}}{\Delta t} \tag{10}$$

However, real signals are rarely completely random in time: they tend to be correlated to the values that came before them. Such *red noise* may be formulated according to Equation 11. Here W_{red} is the new, corrected value for red noise, and r represents the autocorrelation of the wind forcing noise.

$$W_{red}[i] = rW_{red}[i-1] + (1-r)^2 W \tag{11}$$

It is necessary to estimate the values of parameters in the model in order to obtain quantitative results. Based on statistic regression from observational data, reasonable values for each coefficient are chosen and non-dimensionalized by the typical scale of the variables. Among them, the relative coupling coefficient μ can vary from 0 to 1.5, further affecting the values of R and b as the coupling intensity is associated with ocean atmosphere interaction. Detailed arguments for the parameters' values are elaborated in Jin (1997).

Results

We begin by discussing results for the simplest case (Equations 1 and 2), before continuing to those where the non-linear dependence of SST on thermocline depth and annual wind forcing are accounted for. Following this, stochastic forcing is implemented. Then, an ensemble run within a reasonable range of initial conditions is conducted. Finally, spectral analysis is applied to compare the model with the observed NINO3.4 index.

The Simplest Oscillator

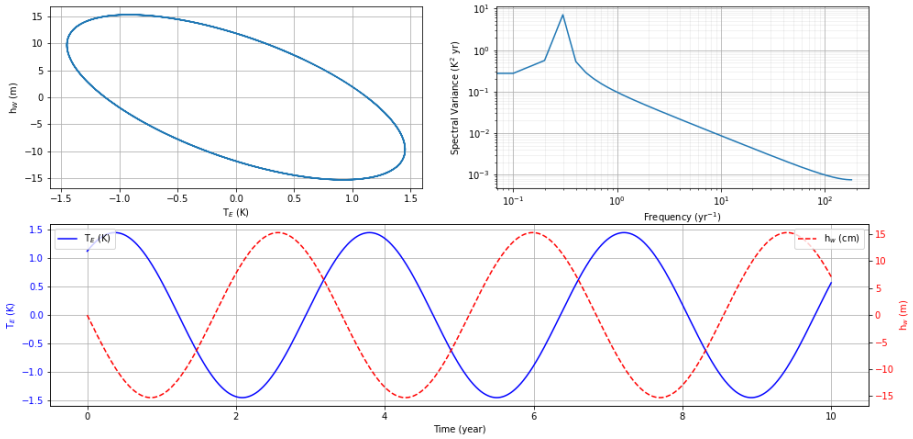

Figure 2: Simple Harmonic Oscillator ENSO Model based on the linearly-coupled equations 1 and 2. From top left in clockwise order: (i) The relationship between T_E and h_W; (ii) the Fourier spectrum of frequency (per year) showing a clear peak at 0.3 yr^{-1} which indicates a typical period of approximately 3 years, 4 months; (iii) the 10-year time series of T_E and h_W. The oscillations are periodic because T_E and h_W are coupled.

Here, Equations 1 and 2 are used and the coupling coefficient μ is 2/3. With initial conditions $T_E = 1.25$ K and $h_W = 0$ m, a harmonic oscillation is seen (Fig. 2). One full cycle takes approximately three years and four months, and there is a roughly six month time lag between the positive maximum of the SST in the East Pacific and the negative maximum of the thermocline depth in the West Pacific. These are both close to the observed data. There is a variation in temperature of about 3K and a thermocline variation of 30m, both

of which are plausible values.

Fundamental features of ENSO variability, the ellipticity of the phase space trajectory, the rotation direction, and the period are well depicted (Fig. 2). More importantly, the rotation trajectory matches the physical dynamics of ENSO. A Fourier spectral analysis of the simulated SST anomaly exhibits the dominant frequency, which is approximately 0.3 yr^{-1} and corresponds to a dominant period of approximately 3.5 years.

The Coupling Coefficient

To what extent the system depends on the coupling coefficient is evident when it is slightly increased or decreased. When the coupling intensity is sufficiently strong ($\mu > 2/3$), the linear growth rate in Equation 1 and 2 becomes positive, and the coupled system manifests as an unstable oscillatory mode. For example, when $\mu = 0.7$, the oscillation explodes (Fig. 3, top).

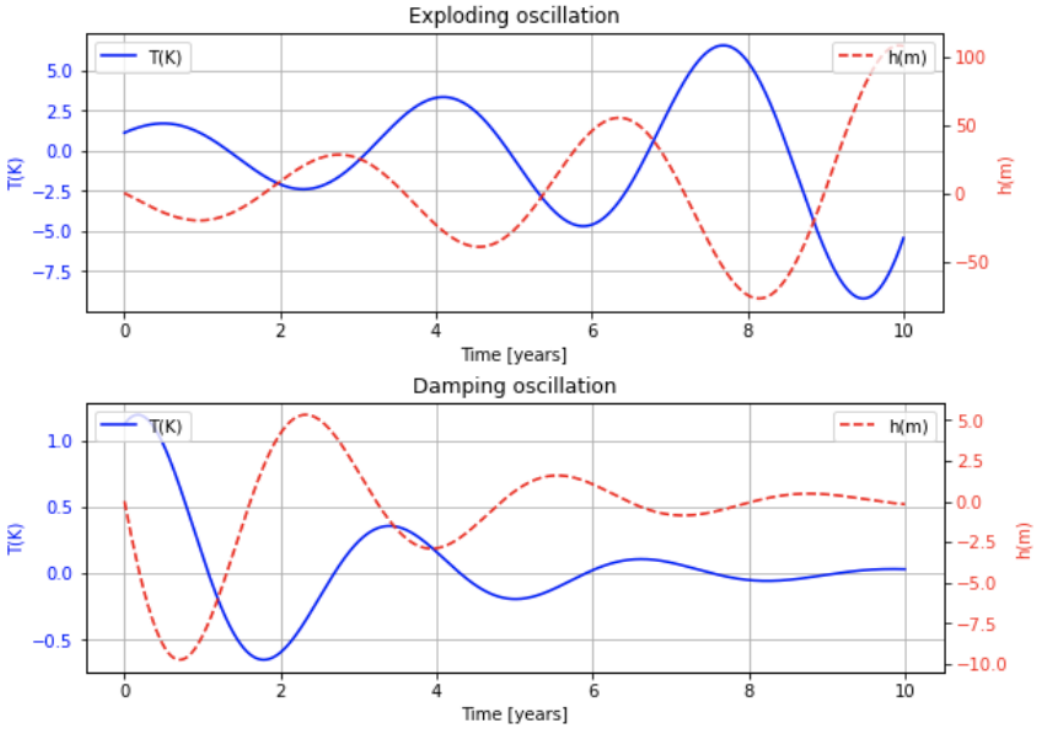

Figure 3: Top plot: $\mu = 0.7$. With a high coupling coefficient μ, the oscillation quickly explodes and reaches unphysical values within two full cycles (approximately eight years). Bottom plot: $\mu = 0.6$. With a low coupling coefficient μ, the oscillation dies away within two periods (approximately seven years).

With sufficiently weak coupling ($\mu < 2/3$), the linear growth rate in Equations 1 and 2 becomes negative, and the coupled system enters a damping oscillatory mode. With $\mu = 0.6$, we can see that the oscillation dies away quite quickly (Fig. 3, bottom).

With a wide range of coupling intensity, the coupled system shows an oscillation mode with a period of 3−5 years. Given values of the parameters discussed above, the dependence of the eigenmodes of the coupled system on the relative coupling coefficient can be solved analytically: it turns out that $\mu = 2/3$ is the critical point. It grows linearly when $\mu > 2/3$, since a strong coupling through Bjerknes feedback results in a growth rate being too

fast to be linearly checked by the slow ocean adjustment. Otherwise, it results in a linear decay when $\mu < 2/3$, as the growth rate decreases rapidly and becomes negative. As will be shown next, adding nonlinearity can limit the linear growth to a self-excited coupled oscillation. A coupled oscillatory solution can also be sustained after taking stochastic forcing into consideration.

Non-Linearity

As the research suggests, a very shallow or very deep thermocline will not linearly increase or decrease the SST anomaly. Non-linearity must therefore be accounted for, and is represented by the non-linear dependence of SST on thermocline depth, which in turn is a reflection of the non-linear vertical distribution of temperature in the tropical ocean (Jin (1997)). It is depicted in Equations 5 and 6 by the term ϵ. Nonlinearity does not alter the

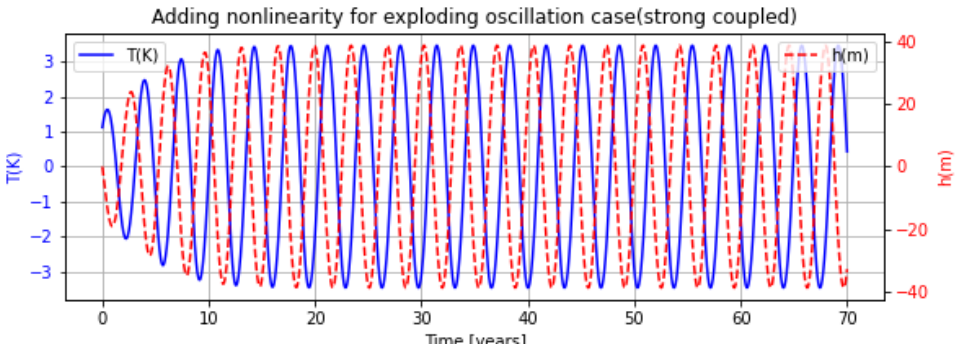

Figure 4: $\mu = 0.7$: after a period of 10 years, the oscillation stabilises. The oscillation is more strongly coupled than in Figure 2 and is as such to a certain extent self-excited and reaches greater amplitudes.

basic dynamics of the recharge oscillator as described by the simplest harmonic oscillation, but does allow for a system that is supercritical to return to a stable oscillation: this may be seen in Figure 4 where despite a larger value for μ, which in the linear case led to exploding values, there is now a 10-year period of slow growth followed by a stable, uniform oscillation.

In this stable state, the amplitudes of both T_E and h_W are now double what they were in the simple, linear state. The oscillation, while stable, is more intense. There is no damping or further growth over the years. The oscillation pattern remains a regular sinusoidal function. However, there is no variation in the duration of El Niño / La Niña events, which is not realistic.

Wind Forcing: An Annual Cycle

The wind stress over the sea surface is critical to ENSO modelling, since it modulates the intensity of thermocline feedback and thus the temporal and spatial distribution of the SST anomaly. Here it is first included in the model through application of Equations 7, 8, and 9. f_{ann} is set to 0.1, and the results for the effect of ξ are shown in Fig. 5.

The large amplitudes and regular periods seen when non-linearity was included are retained (Fig. 4) but there is a new variance in the amplitude, occurring at yearly intervals. Nonetheless, the oscillation is still quite regular and there is little sign of any chaotic behaviour. Since the annual wind force acts as regular weather noise, it cannot represent the realistic chaotic nature of the driving forcing of ENSO variability. As with the previous case, the combination of nonlinearity and weak annual wind forcing leads the system to

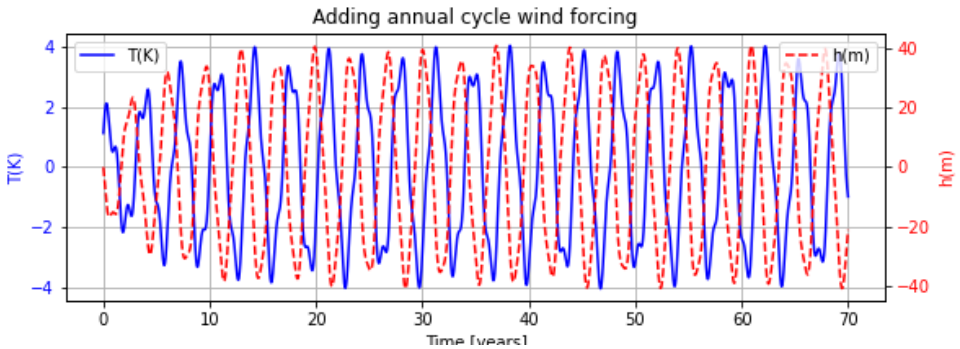

Figure 5: $\mu = 0.7$, $\epsilon = 0.1$: an annual cycle in wind forcing leads to a broader and more irregular range in amplitudes for T_E and h_W. The regular duration is unchanged, however.

grow from its initial conditions before reaching a stable range with peaks (in absolute value) of 3 to 4 K and 30 to 40 m respectively.

Wind Forcing: Stochastic Effects

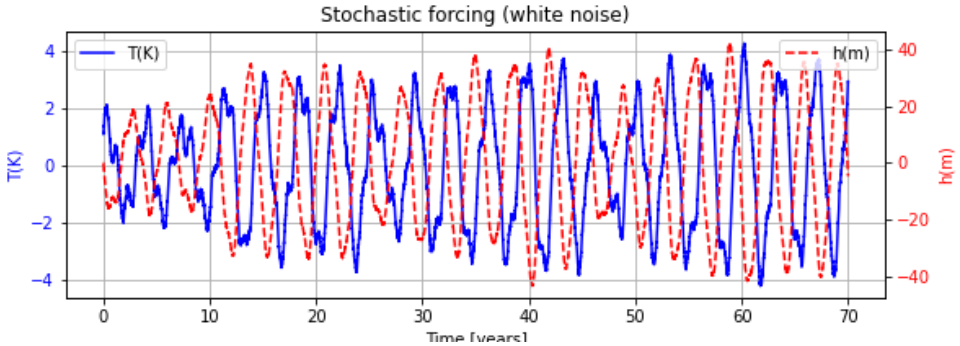

Figure 6: $\mu = 0.7$, $\epsilon = 0.1$, $f_{ran} = 0.4$. Implementation of white noise results in more varied intensities of El Niño / La Niña events but little change in duration.

To analyse the stochastic effect of noise on the wind forcing, Equations 7 and 8 are again used, but Equation 9 is replaced with Equation 10, which introduces randomness to the wind forcing. This randomness is initially white noise, which has zero mean, constant variance, and is uncorrelated in time. Additionally, it has a power spectrum which is uniformly spread across all allowable frequencies. The randomness is accounted for in W which ranges from -1 to 1. The results can show a high frequency daily noise, and the noise amplitude can be adjusted according to the coefficient f_{ran}. The white noise is shown in the model in Figure 6. Here the coefficient is given a higher value to show the difference with respect to the wind forcing model with only a uniform annual cycle. There is now a greater variance in amplitude, with peaks (in absolute value) for T_E and h_W between $2-4$ K and $25-40$ m respectively (not including the initial ten-year period). The duration of individual events does not appear to deviate much from the $3-4$ year period seen before.

Red noise is incorporated using Equation 11 and plotted in Fig. 7. Red noise has zero mean, constant variance, and is serially correlated in time, such that the autocorrelation between two successive time samples has a correlation coefficient $0 < r < 1$. Here the correlation coefficient is set to 0.33. Fig. 7 is quite different to the representation of white noise (Figure 6): the amplitudes overall are much lower and it appears that the duration of particular

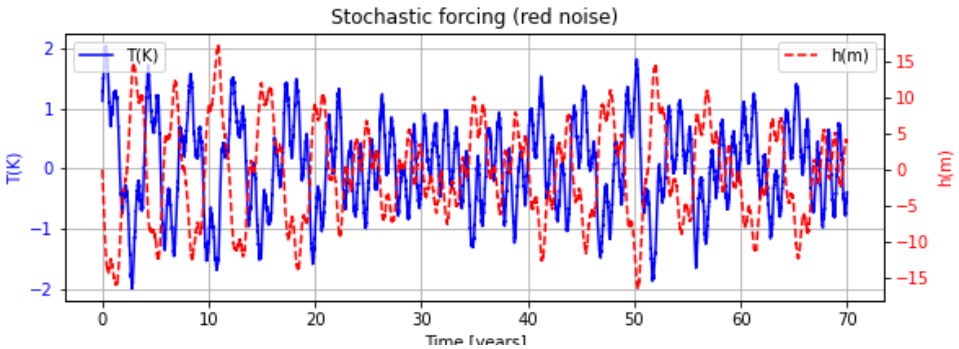

Figure 7: $\mu = 0.7$, $\epsilon = 0.1$: implementation of red noise leads to more chaotic time series. Amplitudes are halved with respect to the nonlinear and white noise analyses. There is also some degree of variance with respect to the period.

events is quite varied. Specifically, peak T_E (in absolute value) range from 0.5−2 K, and peak h_W between 5−15 m. Additionally, it appears that there are some events with long duration (a low-intensity El Niño event from 28−35 years lasting seven years), and others with a quite short duration (a subsequent La Niña event between 35−37 years lasting just two years). Unlike the case with the previous methods, the oscillation does not grow beyond (absolute values of) 2 K or 20 m.

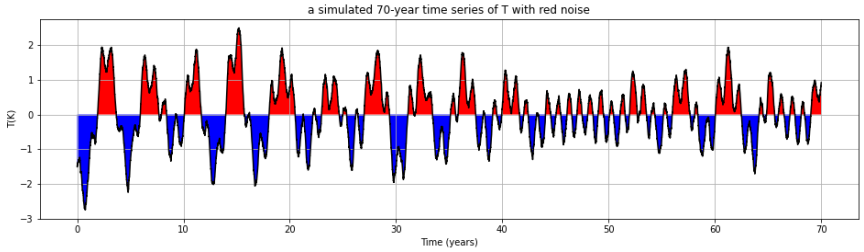

Figure 8: $\mu = 0.75$, $\epsilon = 0.1$: The temperature signal oscillates in irregular periods and amplitudes. This figure is the same as Figure 7 but extended over 70 years and with the thermocline data removed.

For clarity, the model with red noise is plotted again in Fig. 8 where only SST anomaly T_E is shown. This plot is different to before because (i) the initial conditions were chosen to mirror the conditions given by the Oceanic Nino Index for 1950 in Figure 1, and (ii) output for an autocorrelated stochastic model will be different each time it is run due to the growing, autocorrelated noise dependence. The features highlighted before (varying duration, amplitude and trajectory) are still present though.

Ensemble Analysis

To evaluate the effect of stochastic forcing generally, an ensemble analysis for T_E is carried out (Fig. 9). The model is run 50 times across a broad range of initial conditions which are within the amplitude of the oscillation. The initial temperature anomaly ranges from -7.5K to +7.5K, and the initial thermocline depth (not shown) varies from -150m to +150m. Despite the initially broad range, the model shows a damped oscillation which stabilises at a lower range of values. This might be explained by the nonlinearity and noise processes. The absolute value of T_E is typically in the range 1−2.5 K, which is lower than models which consider only non-linear effects or simple annual wind forcing, but of the same order as the stochastically-forced model. This representation may be of limited use in o making

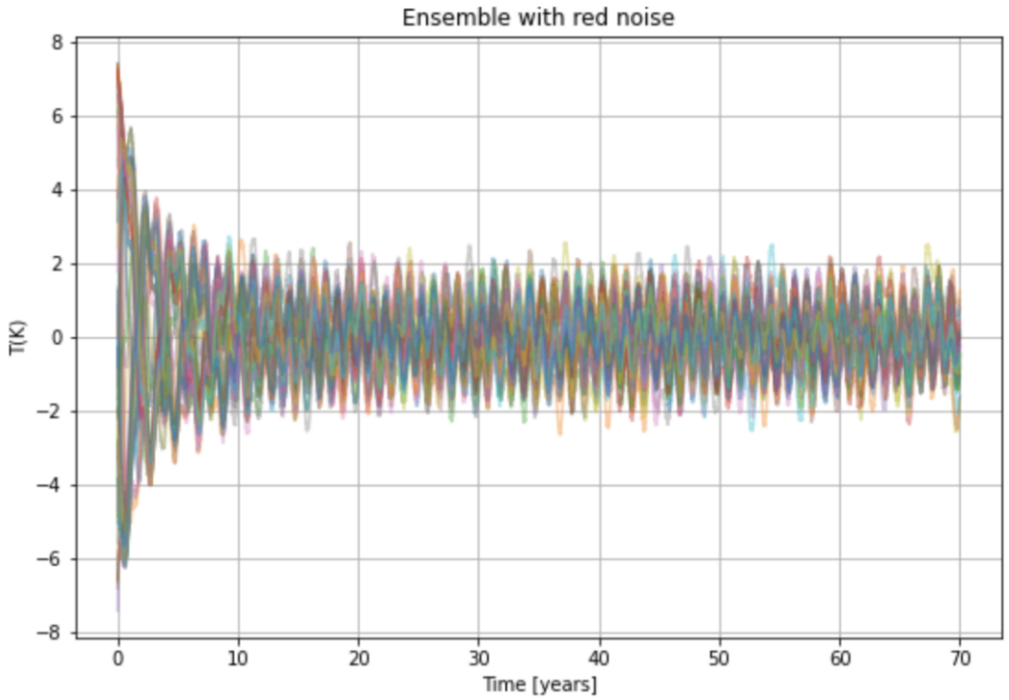

Figure 9: The model is run 50 times as an ensemble. The range of values stabilises following an initial spin-up period. For clarity, only T_E is shown.

predictions. Rather, its usefulness may be in saying that given whatever range of initial conditions the stochastically-forced system will return to a particular balance between a limited set of values.

Comparison to Nino34

Fourier Analysis is carried out on the mean of the ensemble model and Nino34 data (1950−2019). This analysis is shown in Fig. 10, where it is clear that the overall shape of the two data sets match reasonably well. The ensemble has a steeper peak, meaning the range in periods is lower, between 3−5 years. For the NINO3.4 data, the peak is lower, meaning that the range of possible durations is broader (2−7 years) and not so evenly concentrated towards the centre: there are less likely to be a lot of 3-year events. Were the comparison made with a single model run rather than the ensemble mean, it is likely that the peak in ensemble values would not be so sharp.

Conclusion

Overall, it turns out that if the parameters are properly chosen the extended model somewhat resembles the chaotic oscillation pattern of ENSO. Over a wide range of coupling intensity, the model can be self-excited or stochastically sustained with a period of about 3−5 years.

In the most approximate case, the model gives a realistic ENSO of about three years. Irregularity is added to the model through the inclusion of forcing due to non-linearity, wind, and noise. More chaotic time series where El Niño and La Niña phases vary significantly in intensity and duration are obtained in the case where the T and h are somewhat strongly

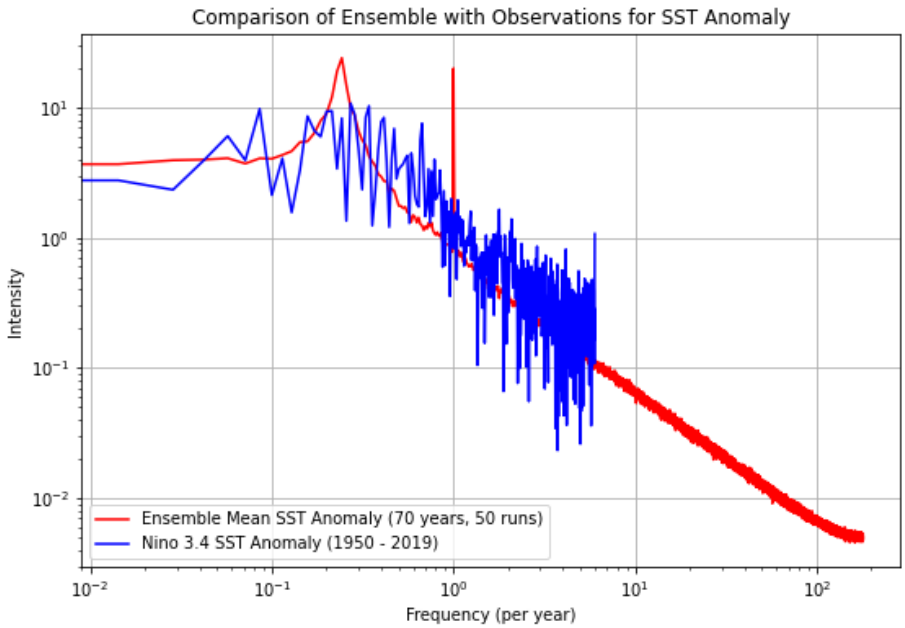

Figure 10: Spectral plot of the ensemble data for stochastically-forced temperature anomaly compared with Nino 3.4 temperature anomaly data. There is a peak in both spectra at approximately 0.3 yr^{-1}, although the range of possible frequencies is broader for the real data.

coupled ($\mu = 0.7$), there is a small degree of non-linearity ($\epsilon = 0.1$), a small degree of annual wind forcing ($f_{ann} = 0.1$), a similarly small degree of random wind forcing ($f_{ran} = 0.2$), and a degree of red noise controlled by an autocorrelation $r = 0.33$.

Whether this model can be used to predict El Niño or La Niña events is not clear. Fig. 8 is initialised with similar initial conditions to ONI (Figure 1), and appears to predict events according to a similar trajectory and with similar duration, at least for a number of cycles, but of less variable amplitude (see also Fig. **??**). Assuming a cut-off of 0.5K in Figure 8, we can also see that the number of events predicted in our model differ, being generally lower for El Niño and higher for La Niña (Our model predicts 16 El Niño and 16 La Niña events, compared to 19 El Niño and 14 La Niña events across a similar time span).

For its simplicity, the model is suprisingly successful, though there are clear issues with the model. El Niño and La Niña are effectively mirror opposites of each other in our model. In reality, they are asymmetrically related: El Niño is more intense, and more frequent. Also, there are other trends that happen in real life that haven't been factored into this model. For instance, La Niña often occurs in consecutive years, a situation that we can see at the moment of writing (November 2021), where it looks as though we are dipping into La Niña for the second year running. This sort of situation rarely occurs with El Niño [An et al (2020)]. Different El Niño types are not recognised in this model either: two particular types of El Niño have been identified in later research [Hsu et al. (2013)].

Future work could consider recent advancements in ENSO knowledge. We could consider parameterisations for different ENSO types, or try to account for the El Niño / La Niña assymmetry.

References

An, S.-I., Tziperman, E., Okumura, Y.M. and Li, T. (2020). ENSO Irregularity and Asymmetry. In El Niño Southern Oscillation in a Changing Climate (eds M.J. McPhaden, A. Santoso and W. Cai). https://doi.org/10.1002/9781119548164.ch7

Bjerknes, J. (1969). Atmospheric Teleconnections from the Equatorial Pacific. Monthly Weather Review, 97, 163-172. https://doi.org/10.1175/1520-0493(1969)097<0163:ATFTEP>2.3.CO;2

Carrillo, C. (1892), Hidrografía oceánica: Las corrientes oceánicas y estudios de la Corriente Peruana ó de Humboldt. Bol Soc Geog Lima 2:72–110

Po-Chun Hsu, Chung-Ru Ho, Shin-Jye Liang, Nan-Jung Kuo, "Impacts of Two Types of El Niño and La Niña Events on Typhoon Activity", Advances in Meteorology, vol. 2013, Article ID 632470, 8 pages, 2013. https://doi.org/10.1155/2013/632470

Jin, F. (1997). An Equatorial Ocean Recharge Paradigm for ENSO. Part I: Conceptual Model, Journal of the Atmospheric Sciences, 54(7), 811-829. Retrieved Nov 11, 2021, from https://journals.ametsoc.org/view/journals/atsc/54/7/1520-$0469_1997_054_0811_aeorpf_2.0.co_2.xml$

Timmermann, A., An, SI., Kug, JS. et al. El Niño–Southern Oscillation complexity. Nature 559, 535–545 (2018). https://doi.org/10.1038/s41586-018-0252-6

Trenberth, Kevin National Center for Atmospheric Research Staff (Eds). Last modified 21 Jan 2020. "The Climate Data Guide: Nino SST Indices (Nino 1+2, 3, 3.4, 4; ONI and TNI)." Retrieved from https://climatedataguide.ucar.edu/climate-data/nino-sst-indices-nino-12-3-34-4-oni-and-tni.

Walker, G. T. (1924) "Correlation in seasonal variations of weather. IX. A further study of world weather," Memoirs of the Indian Meteorological Department, 24 : 275–332.

Wright, P. B., Wallace, J. M., Mitchell, T. P., Deser, C. (1988) “Correlation Structure of the El Niño/Southern Oscillation Phenomenon.” Journal of Climate, vol. 1, no. 6, American Meteorological Society, pp. 609–25, http://www.jstor.org/stable/44365038.